Harmful Algae 8 (2009) 189–195

Contents lists available at ScienceDirect

Harmful Algae

journal homepage: www.elsevier.com/locate/hal

Progress in developing a new detection method for the harmful algal bloom species, *Karenia brevis*, through multiwavelength spectroscopy

Adam H. Spear *, Kendra Daly, Debra Huffman, Luis Garcia-Rubio

University of South Florida, College of Marine Science, 140 7th Avenue South, St. Petersburg, FL 33701, United States

ARTICLE INFO

Article history:
Received 26 July 2007
Received in revised form 2 May 2008
Accepted 6 May 2008

Keywords:
Absorbance
Detection
Harmful algal blooms (HABs)
Karenia brevis
Multiwavelength spectroscopy
Optical properties
Scattering

ABSTRACT

Multiwavelength spectroscopy is a rapid analytical technique that can be applied to detect, identify, and quantify microorganisms such as *Karenia brevis*, the species known for frequent red-tide blooms in Florida's coastal waters. This research will report on a model-based interpretation of UV–vis spectra of *K. brevis*. The spectroscopy models are based on light scattering and absorption theories, and the approximation of the frequency-dependant optical properties of the basic constituents of living organisms. Absorption and scattering properties of *K. brevis*, such as cell size/shape, internal structure, and chemical composition, are shown to predict the spectral features observed in the measured spectra. The parameters for the interpretation model were based upon both reported literature values, and experimental values obtained from live cultures and pigment standards. Measured and mathematically derived spectra were compared to determine the adequacy of the model, contribute new spectral information, and to establish the proposed spectral interpretation approach as a new detection method for *K. brevis*.

1. Introduction

Karenia brevis, a species of toxic dinoflagellate, is known to cause harmful algal blooms (HABs) annually during the late summer and fall in the Gulf of Mexico (Steidinger et al., 1998). Water column toxin levels become more harmful as *K. brevis* increases above background concentrations of 1–1000 cells L^{-1} (Geesey and Tester, 1993). They have the capability to negatively influence fisheries and tourism economies by causing water discoloration (2×10^6 cells L^{-1}), massive fish kills (1.5×10^5 cells L^{-1}), closing of shell fish beds ($>5 \times 10^3$ cells L^{-1}), and inflicting deleterious effects on humans ($>1 \times 10^3$ cells L^{-1}) (Steidinger et al., 1998; Goodwin et al., 2005). To lessen the impact on coastal fisheries and human health through early prediction, there must be complete understanding of the factors which cause HABs. Most importantly, there is a specific need to provide more accurate input for predicting occurrences of HABs by using a multi-platform approach to rapidly obtain data over ecologically relevant spatial and temporal scales (Schofield et al., 1999).

Optical technology such as satellite remote sensing, *in situ* moored optical instruments, and optically equipped autonomous underwater vehicles (AUV) facilitate the ability to obtain data over broad spatial and temporal scales through rapid detection and continuous real-time monitoring. Optical detection of HABs has been limited by the inability to interpret bulk optical signatures of a given water mass and subsequently discriminate a specific phytoplankton species among a mixed community (Millie et al., 1997; Kirkpatrick et al., 2000). Remote sensing technology can monitor HABs over larger spatial areas, however, the inability to detect most HABs without confirmation from other means, lower density detection, lost data due to weather/clouds, and below surface measurements are considered major deficiencies. *In situ* technology, such as moored optical instruments and optically equipped AUVs, address these deficiencies as well as ground truth remote sensing data through rapid detection of a wider range of concentrations of *K. brevis* at or below the surface (Robbins et al., 2006). Fully understanding HAB dynamics require detection of a single HAB species surrounded by mixed communities throughout the water column at a wide range of concentrations (Steidinger et al., 1978).

Optical research has shown *K. brevis* to have distinct spectral characteristics, but studies have yet to fully characterize its spectral properties (Millie et al., 1997; Kirkpatrick et al., 2000; Mahoney, 2001). Using a model implementing the Mie theory, Mahoney (2001) contributed to the understanding of the inherent optical properties of laboratory and natural populations of *K. brevis*. The Mie theory-based model approximated absorption and scattering characteristics based on size distribution, abundance,

* Corresponding author. Tel.: +1 443 521 2220; fax: +1 727 553 1289.
E-mail address: aspear@marine.usf.edu (A.H. Spear).

1568-9883/$ – see front matter © 2008 Elsevier B.V. All rights reserved.
doi:10.1016/j.hal.2008.05.001

absorption thickness, and inferred index of refraction. The absorption thickness and refractive index were approximated from bulk properties of whole cells. Spectral properties were examined throughout the visible spectrum (412–730 nm) with a spectral resolution of 3.3 nm, and in some cases nine total wavelengths. Millie et al. (1997) and Kirkpatrick et al. (2000) developed a method which correlates the fraction of chlorophyll biomass contributed by *K. brevis* and the fourth derivative absorption-based similarity index. This absorption-only analysis of the visible spectrum allowed for the quantification of gyroxanthin-diester, a rare accessory pigment found in only a few dinoflagellate species, which was established as a consistent predictor when correlated with chlorophyll biomass. While previous research has shown significant progress in characterizing the optical properties of *K. brevis*, there is potentially a considerable amount of spectral information not yet reported to date. Several recent studies have proved to be extremely accurate in characterizing spectral properties of a complex microorganism by dividing the cell into multiple components, as well as combining scattering and absorption properties (Alupoaei, 2001; Callahan et al., 2003; Alupoaei and Garcia-Rubio, 2004, 2005; Alupoaei et al., 2004). This includes refractive indices from several chemical components rather than the single estimated refractive index from the whole cell. In addition, it was shown that it is possible to interpret spectral information of microorganisms from a comparably broader wavelength range (220–900 nm) at a resolution of 1 nm (Alupoaei, 2001; Callahan et al., 2003; Alupoaei and Garcia-Rubio, 2004, 2005; Alupoaei et al., 2004). Overall, absorption and scattering properties of a particle, such as cell size/shape, internal structure, and chemical composition, were reported to have a predictable influence over the observed spectrum of several different microorganisms (both eukaryotic and prokaryotic).

Recently, Alupoaei and Garcia-Rubio (2005) formulated an interpretation model for the multiwavelength spectra of microorganisms. The results of Alupoaei and Garcia-Rubio (2005) combined with previous research efforts using the same interpretation model (Alupoaei, 2001; Callahan et al., 2003; Alupoaei and Garcia-Rubio, 2004; Alupoaei et al., 2004) showed that there is a potential for multiwavelength spectroscopy to be used as a rapid analytical technique that can be applied in order to detect, identify, and quantify microorganisms. The modeled spectrum is based on light scattering and absorption theories, and the approximation of the frequency-dependant optical properties of the basic constituents of living organisms. Specifically, the complex structure of the organism was divided into several categories reflecting particular absorption and scattering elements, including the average size of the organism, the average size of the internal structures, the volume fraction of the internal structures and overall chemical composition within the cell. A complex organism was able to be represented through a weighted sum of absorption and scattering components.

The potential exists to reformulate the model proposed by Alupoaei and Garcia-Rubio (2005) to interpret spectra of *K. brevis* through multiwavelength spectroscopy in order to reflect the cellular complexity (Fig. 1) specifically inherent to *K. brevis*. Cellular complexity can be characterized through the identification of unique chemical and physical characteristics of *K. brevis* using multiwavelength spectroscopy, as proven possible by previous research for other microorganisms. Using the proposed model, exploration of unique spectral information not yet reported for *K. brevis* will provide a better understanding of the optical properties, as well as the potential for more accurate and sensitive detection if applied to a deployable instrument.

Due to the success of previous efforts characterizing the scattering and absorption features of the spectra of several different microorganisms (Alupoaei, 2001; Callahan et al., 2003; Alupoaei and Garcia-Rubio, 2004, 2005; Alupoaei et al., 2004), we were subsequently encouraged to apply this method to one of the most ecologically and economically destructive marine organisms in the Gulf of Mexico (Anderson et al., 2000; Magana et al., 2003). In order to interpret experimentally measured spectra, the model proposed by Alupoaei and Garcia-Rubio (2005) has been reformulated to include parameters reflecting the cell structure, size, and chemical composition of *K. brevis*. Modeled spectra were determined using previous literature values, as well as experimentally obtained values using live culture and pigment standards. Experiments were performed using a multiwavelength spectrometer to determine the general variability of spectra. Measured and modeled spectra were compared to determine whether the model is adequate enough for further study and application. The objective of this study was to understand the spectral properties and thereby contribute new spectral information of *K. brevis* using multiwavelength spectroscopy for future application to a more accurate and sensitive detection method.

2. Methods

2.1. Spectroscopy interpretation model

To interpret differences in *K. brevis* spectra, the model proposed by Alupoaei and Garcia-Rubio (2005) was reformulated to include parameters reflecting the complexity of *K. brevis*. The model is based on the measurement of transmitted light. This is done through the use of a broadband light source which is emitted through suspended particles, after which all wavelengths of the transmitted light are measured simultaneously using a multiwavelength spectrophotometer. The model's structure is based on dividing the organism into several distinct components. In this case with *K. brevis*, there are three distinct components that include the main body of the cell, the nucleus, and the chloroplasts. The characteristic dimensions of the macrostructure and internal structures, which include chloroplasts and nucleus, will largely define the scattering properties of the spectrum. The chemical composition, which includes the total nucleotides (DNA + RNA), non-chromophoric protein, and photopigments, will define the absorption properties. The total scattering and absorption components will be given by the weighted sum from the representative components. The equation that relates the turbidity ($\tau(\lambda_0)$) measured at a given wavelength λ_0 and the normalized particle size distribution for spherical particles ($f(D)$) is given by

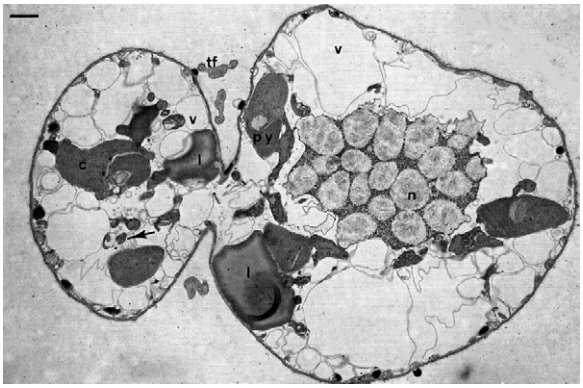

Fig. 1. Transmission electron photomicrograph of a longitudinal section of *K. brevis* from Steidinger et al. (1978). Note the cellular complexity and the different organelles, including the chloroplast (c) and nucleus (n). Scale bar = 1 μm.

(Van Der Hulst, 1957; Kerker, 1969):

$$\tau(\lambda_0) = \mathrm{Np}\, l\left(\frac{\Pi}{4}\right) x \int_0^\infty Q_{\mathrm{ext}}(m(\lambda_0), D) D^2 f(D)\, \mathrm{d}D \quad (1)$$

where D is the effective particle diameter, $Q_{\mathrm{ext}}(m(\lambda_0), D)$ corresponds to the Mie extinction coefficient, l is the path length, and Np is the number of particles per unit volume. The Mie extinction coefficient is a function of the optical properties of the particles and the suspending medium through the complex refractive index ($m(\lambda_0)$) given in Eq. (2):

$$m(\lambda_0) = \frac{n(\lambda_0) + i\kappa(\lambda_0)}{n_0(\lambda_0)} \quad (2)$$

where $n(\lambda_0)$ and $n_0(\lambda_0)$ correspond to the refractive index of the particles and the suspending medium, respectively. The absorption coefficient of the suspended particles is represented by $\kappa(\lambda_0)$. Eq. (1) can be written in matrix form by discretizing the integral with an appropriate quadrature approximation (Elicabe and Garcia-Rubio, 1988, 1990) given by Eq. (3) as

$$\underline{\tau} = A\underline{f} + \underline{\varepsilon} \quad (3)$$

where ε represents a composite of experimental errors, which are errors due to the model approximations and errors introduced by the discretization procedure (Elicabe and Garcia-Rubio, 1990). Eq. (4) gives the regularized solution to Eq. (3) as

$$\underline{\hat{f}}(\gamma) = (A^{\mathrm{T}}A + \gamma H)^{-1} A^{\mathrm{T}}\underline{\tau} \quad (4)$$

where H is a covariance matrix that essentially filters the experimental and the approximation errors (ε from Eq. (3)), and γ is the regularization parameter estimated using the Generalized Cross-Validation technique (GCV) (Golub et al., 1979). The Generalized Cross-Validation technique requires the minimization of Eq. (5) with respect to γ (Golub et al., 1979; Elicabe and Garcia-Rubio, 1990):

$$V(\gamma) = \mathrm{Nob}\frac{|I - A(A^{\mathrm{T}}A + \gamma H)^{-1}\underline{\tau}|^2}{\mathrm{Trace}[I - A(A^{\mathrm{T}}A + \gamma H)^{-1}A^{\mathrm{T}}]^2} \quad (5)$$

where Nob represents the number of discrete turbidity measurements. Eqs. (1)–(5) can be used in a variety of ways depending on the information required and the available data. For example, if the optical properties are known as functions of wavelength, Eqs. (4) and (5) can be used to estimate the particle size distribution. If the particle size distribution is known, from microscopy, Coulter Counter, or other techniques, then Eqs. (1), (2) and (4) can be used to estimate the optical properties, and thus the chemical composition of the particles. Overall, these optical property values are equivalent to a calibration and can be used as fingerprints to classify and identify distinct particle populations (Mattley et al., 2000).

2.2. Experimental

All UV–vis spectra in this study were recorded on an Agilent 8453 diode array spectrophotometer. All spectral measurements in this study were conducted at room temperature using a 1 cm path length, 1 nm resolution, in a 3.5-ml volume quartz cuvette. Prior to measuring the spectrum of each sample the spectrometer were zeroed to account for background light.

The parameters estimated from previous literature values include the average size of the macrostructure, the average size and volume fraction of the internal structures (chloroplasts, nucleus), and the chemical composition in terms of the total nucleotide concentrations, total non-chromophoric proteins, and water content. The case in which the information is unavailable from previous literature, lab experiments and/or educated assumptions was applied. *K. brevis* has one primary photopigment, chlorophyll-*a* (chl-*a*), and several major accessory pigments, including fucoxanthin, diadinoxanthin, and gyroxanthin-diester (Örnólfsdóttir et al., 2003). To better characterize and interpret *K. brevis* cell optical characteristics, a serial dilution of all major characteristic photopigments (chl-*a*, fucoxanthin, gyroxanthin-diester, diadinoxanthin) was performed. Isolated chl-*a* was purchased from Sigma. The remaining accessory pigments were purchased from DHI Water and Environment. The absorption spectra of all pigments were converted to extinction coefficient according to Beer–Lambert law using the known concentration and path length. The refractive index for chl-*a* was estimated from the literature to be 1.52 at 589 nm wavelength (Aas, 1996). The refractive index for the remaining accessory pigments were estimated using additive molar properties method reported in *Properties of Polymers* (Van Krevelen, 1990). All the remaining accessory pigments were found to be near the chl-*a* refractive index value which, for consistency, resulted in the use of 1.52 for all pigments. The extinction spectrum and refractive index of each pigment was then combined to form an optical properties file to be applied to the model.

K. brevis isolate, Apalachicola (C6), was obtained from the Florida Fish and Wildlife Research Institute to observe changes in spectral features over time caused by cell growth and mortality. Culture with an initial concentration 30–60 cells ml^{-1} was held under fluorescent lamps at an irradiance of ~50 μmol quanta $\mathrm{m}^{-2}\,\mathrm{s}^{-1}$ within 14:10 L:D cycles at 24 °C for 2 months. The initial culture consisted of 1.5 l of sterilized filtered seawater and modified general purpose (GSe) medium (Blackburn et al., 2001). The same filtered seawater was also used as a spectral background subtraction. Spectral measurements of *K. brevis* cells were recorded approximately every day, 1–2 times per day. In addition, several field samples of *K. brevis* were taken at Passe-a-Grille beach (west coast of Florida) in late October 2006, to establish the difference of *K. brevis* spectra among natural, mixed populations. Field samples of *K. brevis* were identified by the use of a microscope, and confirmed by the FWRI red tide monitoring website which indicated extremely high concentration blooms in the area (http://research.myfwc.com/). Filtered seawater was used as the background which was subtracted from the sample spectra. This was done using gravity filtering (0.5 μm) to reduce the amount of lysed *K. brevis* cells and subsequent leaking of pigments into the filtrate. After spectral measurement, cell density and size were measured using a Beckman Z2 Coulter Counter, an ocular micrometer, and a Neubauer hemacytometer. The optical density spectra were normalized between 240 nm and 900 nm with their corresponding mean optical density. Normalization allows for the elimination of the effect of the number of particles to cancel and therefore the resulting spectral features can be limited to changes in the size distribution and chemical composition (Alupoaei, 2001). Both *in situ* and culture data were obtained for the purpose of qualitative assessment and to provide a means to determine general progress of the early stages of modeling.

3. Results

Table 1 shows the estimated and literature-obtained values used to model the cell of *K. brevis*. Educated assumptions and/or estimations were utilized for values unobtainable from the literature. The contribution of scattering and absorption to the total optical density spectrum of the modeled chloroplast is shown in Fig. 2. Note the impact of the absorption peaks from the pigments on the total optical density. Typically, isolated chromo-

Table 1
Model parameters: size (μm) and chromophoric concentrations (pg/component)

	Macrostructure	Nucleus	Chloroplasts[a]
Size range	20–40[b]	6–15[b,c]	2–6[b]
Size used	22	10	5.5
Nucleotides range	100–130[c,d]	140–174[c]	0.10–0.40[e]
Nucleotides used	318	200	0.38
Chlorophyll range			0.52–4.91[f,g]
Chlorophyll used			4
Fucoxanthin range			0.19–3.15[f,g]
Fucoxanthin used			2.14
Gyroxanthin range			3.7×10^{-2} to 0.35[g]
Gyroxanthin used			3.7×10^{-2}
Diadinoxanthin range			5.57×10^{-2} to 0.57[g]
Diadinoxanthin used			0.5

Range refers to known literature values. Value used refers to the chosen model parameter values.
[a] Assumed 7 chloroplasts.
[b] Steidinger et al. (1978).
[c] Rizzo et al. (1982).
[d] Calculated from the fraction of DNA/cell given and the amount of DNA/nucleus given by Rizzo et al. (1982).
[e] Estimated.
[f] Evens et al. (2001).
[g] Millie et al. (1995, 1997).

phoric nucleotides have a maximum absorbance band at approximately 260 nm (Freifelder, 1982; Waltham et al., 1994; Tuminello et al., 1997; Alupoaei, 2001). Note in this case that the absorbance feature is slightly shifted to 280–300 nm. This is due to the presentation of the nucleotide absorbance band through a relatively large particle. Several other small spectral features in the UV range can be attributed to the combination of chl-*a*, gyroxanthin-diester, diadinoxanthin, and fucoxanthin. In the region from 350 nm to 550 nm, there is an apparent combination of several different absorbance peaks of chl-*a* (maximum absorbance bands at 410 nm and 430 nm), diadinoxanthin (maximum absorbance bands at 426 nm, 447 nm, 478 nm), and fucoxanthin (maximum absorbance bands at 446 nm and 468 nm) (Jeffrey et al., 1997). In addition, gyroxanthin-diester has distinct absorbance peaks in this region as proven by known maximum absorbance bands at 421 nm, 446 nm, and 468 nm (Millie et al., 1995). Chlorophyll-*a* has additional maximum absorbance bands at approximately 618 nm and 660 nm (Jeffrey et al., 1997). The

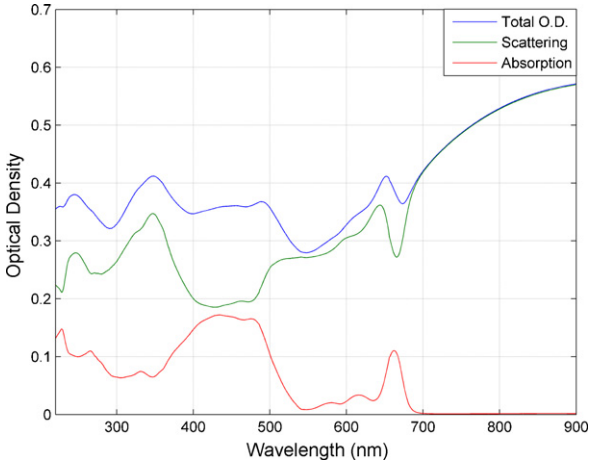

Fig. 2. The contribution of scattering and absorption to the total optical density spectrum of the modeled chloroplast. Note the contribution of the combination of the absorbance bands of chl-*a*, diadinoxanthin, fucoxanthin, and gyroxanthin-diester from 350 nm to 550 nm. Chlorophyll-*a* has additional absorbance bands between 600 nm and 700 nm.

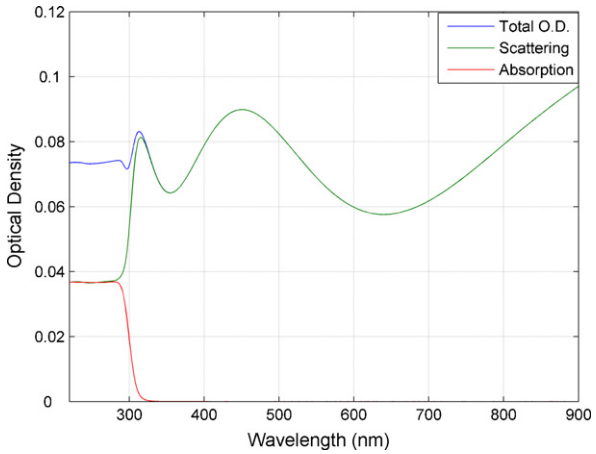

Fig. 3. The modeled nucleus and the contribution of scattering and absorption to the total optical density spectrum. Notice the absorption bands from 280 nm to 350 nm resulting from nucleotides in combination with scattering. The scattering from the relatively large nucleus (10 μm) dominates the visible wavelengths.

overall theoretical estimation of the combination of scattering from a 5.5-μm particle and the absorption bands from the pigments demonstrates a unique spectral signature.

The modeled nucleus and its contribution to scattering and absorption to the total optical density spectrum are shown in Fig. 3. The spectral properties in the UV range are influenced the most by the absorption from nucleotides, as seen by the peek around 280–350 nm. In contrast, the visible wavelength range is dominated by the scattering from the size of the relatively large nucleus (10 μm). The large feature from 400 nm to 600 nm and the gradual rise in optical density from 650 nm to 900 nm are both the result of scattering.

An example of spectra calculated for the body of the cell (macrostructure) is also shown (Fig. 4). As in the case of the nucleus, scattering dominates the visible portion of the spectra. The nucleotide contribution to absorption is also apparent in the UV portion (280–320 nm) of the spectrum. This is expected given the large absorption coefficients of the nucleotides.

The calculated total optical density for *K. brevis* and the contribution from each of the components are shown (Fig. 5). Clearly, the spectral features contributed by each modeled

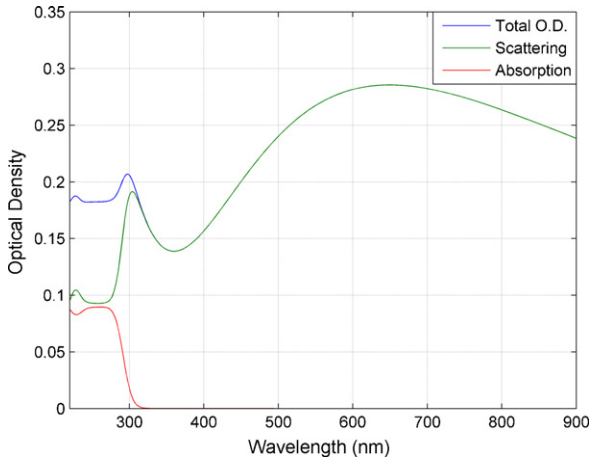

Fig. 4. The spectral interpretation of the macrostructure and the contribution of scattering and absorption to the total optical density spectrum. Notice the absorption bands from 280 nm to 320 nm resulting from nucleotides in combination with scattering. Scattering dominates the visible wavelengths.

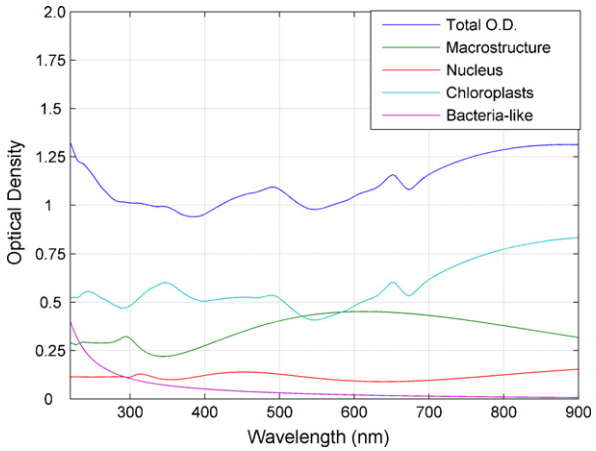

Fig. 5. The calculated total optical density for *K. brevis* and the contribution from each of the components. The spectral features contributed by each modeled component, specifically the chromophoric groups, have a significant effect on the total optical density.

component, specifically the chromophoric groups, have a significant effect on the total optical density. Note the overall contribution from each population over different portions of the spectra and the similarities with the measured spectra.

Dinoflagellate–bacteria interactions can include bacteria that are free-living, attached to the cell, or intracellular (Jasti et al., 2005; Snyder et al., 2005). Typical spectral features of bacteria (*E. coli* for example) will exhibit a large peak from approximately 200 nm to 280 nm, in addition to a nucleotide absorbance feature around 260 nm, followed by a steady decrease in optical density into the visible region (Alupoaei, 2001; Alupoaei and Garcia-Rubio, 2004, 2005). It is debatable whether bacteria will have a significant measurable contribution to the overall optical density due to their likely low concentration. In any case, this particular generalized "bacteria-like" feature seemed to be a missing spectral property and, therefore, was estimated as intracellular and applied to the model. It is worth noting that there are other cellular scenarios which need to be explored that would have results similar to bacteria. Notice that spectral features of bacteria have a considerable influence on the UV region.

To illustrate corresponding spectral changes over time, the data from the culture experiments were split into the lag, log, and stationary phases of growth (Fig. 6). Within the log phase, there is a noticeable gradual progression of an increase in scattering from 400 nm to 900 nm over time. This increase in scattering is likely due to the corresponding average increase in cell size, as larger particles tend to forward scatter longer wavelengths. Another explanation for the gradual increase in optical density from 400 nm to 900 nm could be a corresponding increase in non-chromophoric protein or lipids over time. On average, the cell wall could be thickening or the amount of lipids could be increasing, etc., as the cell gets older resulting in an increase in scattering. An increasing average cell size can also be an explanation for the decrease in optical density from 240 nm to 340 nm. As the average cell size increases, the amount of light that passes through for measurement decreases hence the decrease in optical density. This is a case where the wavelength is much smaller than the particle itself, such that, a shadow effect is created. An increase in organelle size or number can also result in a decrease in the amount of light that passes through. Overall, note that each phase has its own distinct spectral signature. For example, note the dramatic difference between stationary/death and the lag/log phase across the entire spectrum. This difference among phases can be assumed to be attributed to the fact that in stationary and death phase the number of dead or dying cells will increase. Specifically, the dead or decaying cells break up and reintroduce proteins and lipids back into the water column and are subsequently measured along with live cells. A large absorption peak around 240–300 nm, followed by sharp decline around 350–400 nm, and a gradual decrease in scattering from 400 nm to 900 nm are typical spectral features of small particles consisting of mostly protein and water; an example of this would be a typical bacteria spectrum (Alupoaei, 2001; Alupoaei and Garcia-Rubio, 2004, 2005). In summary, it is worth observing the variability that is presented throughout the growth cycle.

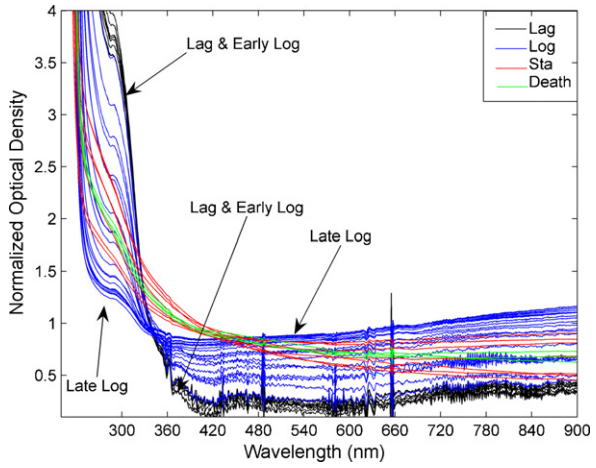

Fig. 6. To illustrate corresponding spectral changes over time, the culture experiment data was split into the lag, log, and stationary phases of growth. Note that each phase has its own distinct spectral signature.

There is a noticeable difference between the cultured and *in situ* spectra in the UV region (Figs. 6 and 8). Since the *in situ* measurement was microscopically determined to be primarily a monospecific bloom of *K. brevis,* the difference between the cultured and *in situ* spectra is most likely a result of different sampling techniques. Due to the variability of seawater as a background subtraction in the *in situ* sample, only the filtered seawater from the same sample could be used. There is a strong possibility that some cell debris, proteins, etc. did in fact make it through the filter and subsequently subtracted from the sample spectrum resulting in more defined features in the UV region. In the case of the culture sampling, for consistency, the exact seawater used to start the culture was also subtracted throughout the growth cycle. It is likely that this seawater is much cleaner because it was not obtained from the bloom, and therefore cell debris, protein, etc. were not subtracted. It is worth mentioning that the media spectrum was not subtracted from the sample spectra because of the complete lack of spectral features after 240 nm and therefore had little relevancy. Therefore, due to the likelihood that the *in situ* samples are a more accurate spectral signature when compared to the culture samples, they were used as a representative spectral fingerprint to be compared to the modeled spectra. When the calculated and measured *in situ* spectra are compared, several of the main features are consistent (Figs. 7 and 8). As it can be appreciated in both plots, arrows A and B are pointing to the features involved in the combination of nucleotides and accessory pigments. Arrow C indicates the contribution of scattering and absorption from chl-*a* and the accessory pigments. Arrow D is pointing to the combination from scattering from the cell and absorption from chl-*a*. Overall, the theoretical predictions reproduce the main features of the measured spectra and therefore offer the possibility of identifying a fingerprint for *K. brevis.*

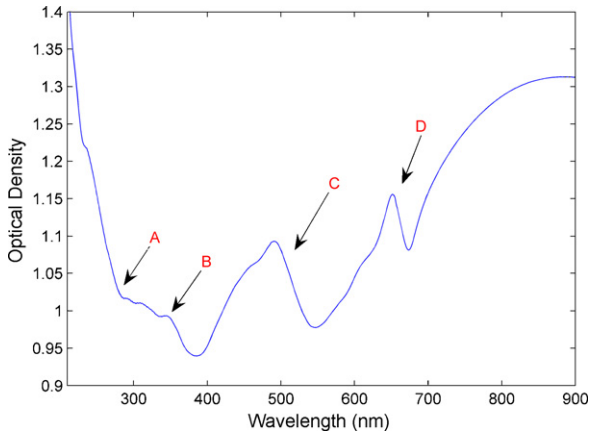

Fig. 7. Modeled total optical density spectrum for *K. brevis*. Arrows A and B point to the features involved in the combination of nucleotides and accessory pigments. Arrow C points to the contribution of scattering and absorption from chl-*a* and accessory pigments. Arrow D points to the combination from scattering from the cell and absorption from chl-*a*.

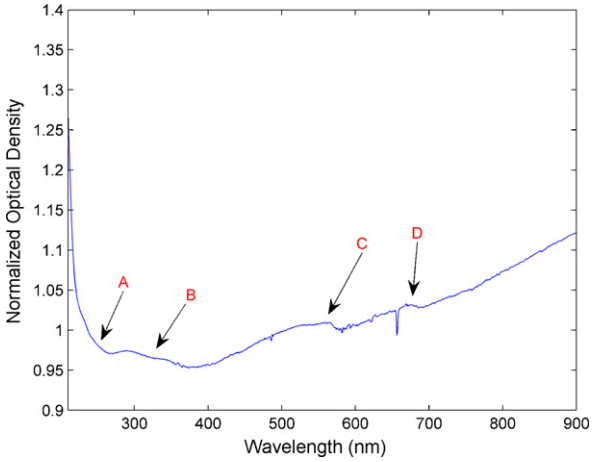

Fig. 8. Measured normalized total optical density spectrum for *K. brevis* from *in situ* sample collection. Arrows A and B point to the features involved in the combination of nucleotides and accessory pigments. Arrow C indicates the contribution of scattering and absorption from chl-*a* and the accessory pigments. Arrow D points to the combination from scattering from the cell and absorption from chl-*a*.

4. Discussion

The results described in the previous section demonstrate that despite the apparent difference between measured and predicted spectra, a considerable amount of progress has been made on the understanding of the spectral features of *K. brevis*. It is now possible to predict with some degree of accuracy what parameter, based on both absorption and scattering components, is responsible for each feature in the observed *in situ* spectra. Representation of pigment composition within the chloroplast, combined with physical features, show significant influence on the total optical density of the whole cell. Influence from the nucleotide content from the macrostructure and nucleus, combined with physical features, are also apparent in the total optical density.

This method which utilizes every spectral feature given by the interaction of light with the cellular components and their contribution to the total spectrum of *K. brevis* is reported for the first time. Previous optical studies of *K. brevis* were limited as a result of disregarding the ultraviolet wavelength portion of the spectrum and the use of only the absorption properties of the main chromophores. Whenever scattering was included in the description of spectral features, only the bulk properties of the cell were considered (Millie et al., 1997; Kirkpatrick et al., 2000; Mahoney, 2001). The approach of splitting the cell into multiple components allows for the spectral properties of a complex organism to be characterized at a much more detailed and therefore sensitive level. Utilizing the ultraviolet portion of the spectrum allows for an increased degree of sensitivity with the ability to characterize additional spectral features such as cell size, and nucleotide and protein concentration. The proposed model offers the possibility of exploring the sensitivity of the measurement to as many cellular components as determined to be necessary by the researcher. As a result, the potential for a high level of characterization of the cell increases the possibility of separating a similar species of the same genus. This is an important attribute due to the findings of Heil et al. (in press) which documented at least four other known Karenia species besides *K. brevis* and *Karenia mikimotoi* in a *K. brevis* dominated bloom in the Gulf of Mexico. All six species were found to co-occur during a 2005 bloom in the Gulf of Mexico, with *K. brevis* dominating total *Karenia* abundance from bloom initiation to termination, on average comprising over 81% of *Karenia* cells in each sample. The second most dominant species, *K. mikimotoi*, still reached significant concentration levels of 10^7 cells L^{-1}. It was also found that five other less abundant species showed unique differences in spatial and temporal distribution. The ecological impact of species co-occurring with *K. brevis* will depend on concentration and toxicity but will ultimately remain unknown until better monitoring technology is developed. To our knowledge, neither study which focused on *K. brevis* detection has yet to report or attempt to detect them among similar species of the same genus (Millie et al., 1997; Kirkpatrick et al., 2000; Robbins et al., 2006).

Future studies will need to focus on the major physiological and chemical factors, such as cell division, cell size/shape, motility, and chromophoric components, in order to accurately characterize and interpret spectra of *K. brevis*. For example, *K. brevis* is positively phototactic, which results in almost immediate vertical movement (cell swim speeds range, depending on the strain, from ~209 $\mu m\ s^{-1}$ to 358 $\mu m\ s^{-1}$) towards the sea surface in response to sunlight (Steidinger et al., 1998; McKay, 2004). Cells must acclimate to high or low irradiances (UV–vis) resulting in a change in chemical structure for protection or energy (Millie et al., 1995; Kirkpatrick et al., 2000; Evens et al., 2001). Accessory pigment amounts are also known to change between strains of *K. brevis* adding to the variability (Bjornland et al., 2003). In all, cells may give different spectral signals due to time of day, response to emitted light during the measurement, cell growth, and cell division. Once all researched variables are considered and applied, a statistical analysis will be needed to determine the sensitivity of the model and the range of spectral variability.

Instrument sensitivity was a limiting factor in this study and will need to be addressed in future studies. Due to a large cell size (15–30 μm diameter), *K. brevis* creates significant scattering which leads to less obvious absorption features within the spectrum. This problem can be alleviated through an increase in path length, along with the use of a more powerful light source, which will result in more defined absorption features.

The purpose of this research is to investigate the optical spectroscopy of *K. brevis* in order to understand its spectral characteristics. It has been shown that the proposed model is capable of predicting the spectral features of *K. brevis*. It can be expected that the differences between the interpreted and measured spectra can be reduced as better estimates of the optical properties become available. In recent years, technology has advanced such that multiwavelength spectrophotometers are

almost as small as a cell phone and thus easily deployable for rapid analytical measurement. Advancing spectrophotometer technology, in combination with the proposed interpretation model, should eventually prove to address the detection deficiencies of current optical applications and facilitate the understanding of *K. brevis* bloom ecology.

Acknowledgements

This research was supported by funding from Claro Scientific, LLC, St. Petersburg, FL.[SS]

References

Aas, E., 1996. Refractive index of phytoplankton derived from its metabolite composition. J. Plankton Res. 18 (12), 2223–2249.
Alupoaei, C.E., 2001. Modeling of the transmission spectra of microorganisms. Master of Science Thesis. University of South Florida.
Alupoaei, C.E., Garcia-Rubio, L.H., 2005. An interpretation model for the UV–vis spectra of microorganisms. Chem. Eng. Commun. 192, 198–218.
Alupoaei, C.E., Garcia-Rubio, L.H., 2004. Growth of behavior of microorganisms using UV–vis spectroscopy: *Escherichia coli*. Biotechnol. Bioeng. 85 (2), 163–167.
Alupoaei, C.E., Olivares, J.A., Garcia-Rubio, L.H., 2004. Quantitative spectroscopy analysis of prokaryotic cells: vegetative cells and spores. Biosens. Bioelectron. 19, 893–903.
Anderson, D.M., Hoagland, P., Kaoru, Y., White, A.W., 2000. Estimated annual economic impacts from harmful algal blooms (HABs) in the United States. Woods Hole Oceanographic Institute. Technical Report, WHOI-2000-11.
Bjornland, T., Haxo, F.T., Liaaen-Jensen, S., 2003. Carotenoids of the Florida red tide dinoflagellate *Karenia brevis*. Biochem. Syst. Ecol. 31, 1147–1162.
Blackburn, S.I., Bolch, C.J.S., Haskard, K.A., Hallegraeff, G.M., 2001. Reproductive compatibility among four global populations of the toxic dinoflagellate *Gymnodinium catenatum* (Dinophyceae). Phycologia 40 (1), 78–87.
Callahan, M.R., Rose, J.B., Garcia-Rubio, L., 2003. Use of multiwavelength transmission spectroscopy for the characterization of *Cryptosporidium parvum* oocysts: quantitative interpretation. Environ. Sci. Technol. 37 (22), 5254–5261.
Elicabe, G., Garcia-Rubio, L., 1988. Latex particle size distribution from turbidimetric measurements combining regularization and Generalized Cross-Validation techniques. J. Colloid Interface Sci. 129, 192–200.
Elicabe, G., Garcia-Rubio, L., 1990. Latex particle size distribution from turbidimetry using a combination of regularization techniques and generalized cross-validation. Adv. Chem. Ser. 227, 83–104.
Evens, T.J., Kirkpatrick, G., Millie, D., Chapman, D., Schofield, O., 2001. Photophysiological responses of the toxic red-tide dinoflagellate *Gymnodinium breve* (Dinophyceae) under natural sunlight. J. Plankton Res. 23 (11), 1177–1193.
Freifelder, D., 1982. Physical Biochemistry, 2nd ed. W.H. Freeman and Company, 504 pp. (Chapter 14).
Geesey, M.E., Tester, P.A., 1993. *Gymnodinium breve*: ubiquitous in Gulf of Mexico waters? In: Smayda, T.J., Shimizu, Y. (Eds.), Toxic Phytoplankton Blooms in the Sea. Elsevier, Amsterdam, pp. 251–255.
Golub, G.H., Heath, M., Wahba, G., 1979. Generalized Cross-Validation as a method for choosing a good ridge parameter. Technometrics 21, 215–223.
Goodwin, K.D., Cotton, S.A., Scorzetti, G., Fell, J.W., 2005. A DNA hybridization assay to identify toxic dinoflagellates in coastal waters: detection of *Karenia brevis* in the Rookery Bay National Estuarine Research Reserve. Harmful Algae 4, 411–422.
Heil, C., Truby, E., Wolny, J., Pigg, R., Richardson, B., Garrett, M., Haywood, A., Petrik, K., Flewelling, L., Stone, E., Cook, S., Scott, P., Steidinger, K., Landsberg, J., in press. The multi-species nature of the 2005 *Karenia* bloom in the eastern Gulf of Mexico. In: Proceedings of the 12th International Conference on Harmful Algae.
Jasti, S., Sieracki, M.E., Poulton, N.J., Giewat, M.W., Rooney-Varga, J.N., 2005. Phylogenetic diversity and specificity of bacteria closely associated with *Alexandrium* spp. and other phytoplankton. Appl. Environ. Microbiol. 71 (7), 3483–3494.
Jeffrey, S.W., Mantoura, R.F.C., Bjørnland, T., 1997. Data for the identification of 47 key phytoplankton pigments. In: Jeffrey, S.W., Mantoura, R.F.C., Wright, S.W. (Eds.), Phytoplankton Pigments in Oceanography: Guidelines to Modern Methods. UNESCO, Paris, pp. 449–559.
Kerker, M., 1969. The Scattering of Light and Other Electromagnetic Radiation. Academic Press, New York.
Kirkpatrick, G.J., Millie, D.F., Moline, M.A., Schofield, O., 2000. Optical discrimination of a phytoplankton species in natural mixed populations. Limnol. Oceanogr. 45 (2), 467–471.
Magana, H., Contreras, C., Villareal, T.A., 2003. A historical assessment of *Karenia brevis* in the western Gulf of Mexico. Harmful Algae 2 (3), 163–171.
Mahoney, K., 2001. Optical properties of *Karenia brevis* and implications for remote sensing reflectance. Ph.D. Dissertation. University of Southern Mississippi.
Mattley, Y., Leparc, G., Potter, G., García Rubio, L., 2000. Light scattering and absorption model for the quantitative interpretation of human platelet spectral data. Photochem. Photobiol. 71 (5), 610–619.
Millie, D.F., Kirkpatrick, G.J., Vinyard, B.T., 1995. Relating photosynthetic pigments and in vivo optical density spectra to irradiance for the Florida red-tide dinoflagellate *Gymnodinium breve*. Mar. Ecol. Prog. Ser. 120, 65–75.
Millie, D.F., Schofield, O.M., Kirkpatrick, G.J., Johnsen, G., Tester, P.A., Vinyard, B.T., 1997. Detection of harmful algal blooms using photopigments and absorption signatures: a case study of the Florida red tide dinoflagellate *Gymnodinium breve*. Limnol. Oceanogr. 42 (5), 1240–1251.
McKay, L.L.E., 2004. *K. brevis* cells' swimming speeds and internal cellular states over a range of temperatures and light intensities. Master's Thesis. North Carolina State University.
Örnólfsdóttir, E.B., Pinckney, J.L., Tester, P.A., 2003. Quantification of the relative abundance of the toxic dinoflagellate, *Karenia brevis* (Dinophyta), using unique photopigments. J. Phycol. 39 (2), 449–457.
Robbins, I.C., Kirkpatrick, G.J., Blackwell, S.M., Hillier, J., Knight, C.A., Moline, M.A., 2006. Improved monitoring of HABs using autonomous underwater vehicles (AUV). Harmful Algae 5 (6), 749–761.
Rizzo, P.J., Jones, M., Ray, S.M., 1982. Isolation and properties of isolated nuclei from the Florida red tide dinoflagellate *Gymnodinium breve* (Davis). J. Protozool. 29 (2), 217–222.
Schofield, O., Grzymski, J., Bisset, W.P., Kirkpatrick, G.J., Millie, D.F., Moline, M., Roesler, C.S., 1999. Optical monitoring and forecasting for harmful algal blooms: possibility or pipe dream? J. Phycol. 35 (6), 1477–1496.
Snyder, R.V., Guerrero, M.A., Sinigalliano, C.D., Winshell, J., Perez, R., Lopez, J.V., Rein, K.S., 2005. Localization of polyketide synthase encoding genes to the toxic dinoflagellate *Karenia brevis*. Phytochemistry 66 (15), 1767–1780.
Steidinger, K.A., Truby, E.W., Dawes, C.J., 1978. Ultrastructure of the red tide dinoflagellate *Gymnodinium breve*. I. General description. J. Phycol. 14 (1), 72–79.
Steidinger, K.A., Vargo, G.A., Tester, P.A., Tomas, C.R., 1998. Bloom dynamics and physiology of *Gymnodinium breve* with emphasis on the Gulf of Mexico. In: Anderson, D.M., Cembella, A.D., Hallegraeff, G.M. (Eds.), Physiological Ecology of Harmful Algal Blooms. Springer-Verlag, Berlin, pp. 133–153.
Tuminello, P.S., Arakawa, E.T., Khare, B.N., Wrobel, J.M., Querry, M.R., Milham, M.E., 1997. Optical Properties of *Bacillus subtilis* from 0.2 to 2.5 μm. Appl. Optics 36 (13), 2818–2823.
Van Der Hulst, H., 1957. Light Scattering by Small Particles. Wiley, New York.
Van Krevelen, D.W., 1990. Properties of Polymers: Their Correlation with Chemical Structure, their Numerical Estimation and Prediction from Additive Group Contributions, 3rd ed. Elsevier, New York.
Waltham, C., Boyle, J., Ramey, B., Smit, J., 1994. Light scattering and absorption caused by bacterial activity in water. Appl. Optics 33, 7536–7540.